THE JOURNAL OF PHYSICAL CHEMISTRY C LETTERS

2008, *112,* 11609–11613
Published on Web 07/11/2008

Polarization-Dependent Surface Enhanced Raman Scattering from Silver 1D Nanoparticle Arrays

Wei Luo,[†,‡] Wytze van der Veer,[†] Ping Chu,[‡] D. L. Mills,[‡] Reginald M. Penner,[†] and John C. Hemminger*[,†]

Department of Chemistry, University of California, Irvine, Irvine, California 92697-2025, and Department of Physics and Astronomy, University of California, Irvine, Irvine, California 92697-4575

Received: April 21, 2008; Revised Manuscript Received: June 17, 2008

Arrays of linear, one-dimensional (1D) silver nanoparticle rows have been synthesized that demonstrate strong surface enhanced Raman scattering (SERS) that is dependent on the polarization of the incident electromagnetic radiation. Ordered arrays of 1D rows of spherical silver nanoparticles were fabricated on highly oriented pyrolytic graphite (HOPG) by physical vapor deposition (PVD) at 400 °C. Scanning electron microscopy confirmed the formation of arrays of highly parallel rows of nanoparticles. The rows are typically hundreds of microns long with particle gaps less than 10 nm and 10−1000 nm spacing between adjacent 1D rows. The polarization dependence of the SERS was characterized using thiophenol as a Raman probe molecule that was adsorbed as a monolayer on the silver nanoparticle surfaces. When incident light is polarized along the axis of the nanoparticle rows, the intensity of the Raman-scattered light was ≈20 times stronger than Raman scattered light when the incident radiation was polarized perpendicular to the axis of the nanoparticle rows. This polarization selectivity is in good agreement with our calculations that explore the electromagnetic response of the interacting nanoparticles with an incident light field.

Surface enhanced Raman scattering (SERS) is particularly interesting for its potential in the development of chemical sensing, new analytical devices, and single molecule detection.[1] This interest drives concurrent research into the fabrication and characterization of new nanostructures that demonstrate exceptional SERS activity. One especially promising method involves fabrication of metal nanostructures with nanoscale gaps that can carry strong and localized surface plasmon resonances leading to local field enhancements of $10^{14}-10^{15}$.[2,3] These gaps, known as "hot spots", have been explored mainly in the context of metallic nanoparticle dimers and aggregated colloids. These structures provide strong SERS signals but the complexity and irregularity of these dimers and aggregates present difficulties for correlating the scattering enhancements to the specific "hot spot" morphology.[4,5] Additionally, the polarization dependence of SERS in Ag nanoparticle dimers,[6] in-line aligned Ag nanorods,[7] and coupled metallic nanowires[8,9] indicate that strong enhanced electromagnetic fields preferably locate in the nanostructure interstices that are in the sub-10-nm range.[10–14] However, there remains a need to consistently synthesize organized nanostructures that demonstrate strong polarization-dependent SERS activity and that are highly ordered over length scales that are easily addressed optically. Polarized SERS experiments have the potential to elucidate fundamental aspects of molecule−surface interactions including physical orientation or chemical interactions.[15–17] This research yields a deeper insight into the SERS phenomenon itself and potentially provides an invaluable tool for surface science-based analysis of single molecules and biomolecule detection.[18]

In this letter, we report the fabrication of highly ordered arrays of parallel rows of Ag nanoparticles on HOPG substrates by physical vapor deposition (PVD). These arrays are characterized by scanning electron microscopy (SEM) and their polarization effects are explored through the Raman scattering of thiophenol adsorbed to the nanoparticles. These arrays exhibit strong SERS scattering that is dependent on the polarization of the incident light. We also model the observed experimental results with theoretical calculations that model the localized electric field around these nanoparticles when they are excited by incident light. The calculated results are consistent with experimental results and provide insight into the origin of the polarization dependence of the enhancement.

Arrays of one-dimensional rows of silver nanoparticles were prepared by physical vapor deposition of silver onto highly oriented pyrolytic graphite (HOPG) surfaces. The parallel arrays of linear step edges naturally present on freshly cleaved HOPG surfaces served to template the nucleation of silver, as previously described.[19] Briefly, HOPG substrates were cleaved in air, mounted on sample holders, and immediately inserted into an Edwards 306A thermal evaporation coating system. The chamber pressure was evacuated below 10^{-6} Torr and the HOPG substrates were heated to and maintained at 400 °C for 4 h to remove water from the surface. Following cleaning, Ag deposition was carried out with the HOPG held at 400 °C, which is higher than deposition temperatures previously reported in the literature.[20] A FTM5 film thickness monitor (Edwards, U.K.) was used to measure the deposition rate and mass thickness of the Ag reaching the HOPG surfaces. Silver (Alfa Products, grade

* To whom correspondence should be addressed. E-mail: jchemmin@uci.edu.
† Department of Chemistry, University of California, Irvine.
‡ Department of Physics and Astronomy, University of California, Irvine.

10.1021/jp803455s CCC: $40.75

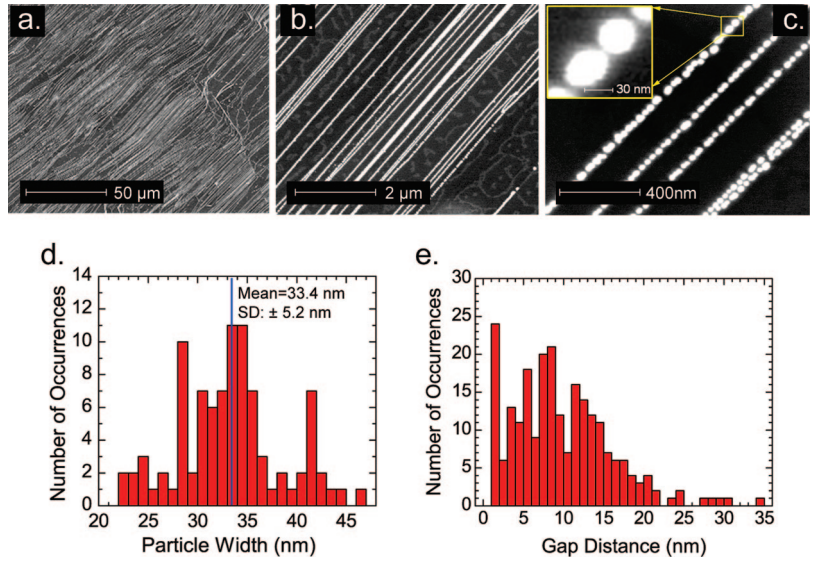

Figure 1. SEM images of Ag nanoparticle arrays on a HOPG substrate grown at 400 °C deposition temperature with 5.5 nm mass thickness of silver. (a), (b), and (c) are images with different scales. (d) and (e) show the distributions of the particle width and the gap sizes obtained from the SEM images.

6N) was deposited to an equivalent uniform thickness of 5.5 nm with a deposition rate of 0.24 Å/s generating the characteristic nanostructures shown in Figure 1. Under these deposition conditions, the Ag atom mobility was sufficiently high that silver particle nucleation only occurred at the atomic step edges present on the HOPG surface. The localization of the nucleation at the HOPG step edges results in the growth of rows of Ag nanoparticles. The arrays of 1D silver nanoparticle rows prepared using this approach follow the atomic step edges on the HOPG surface which are extremely long (>100 μm), approximately straight and organized into parallel arrays of thousands of steps. X-ray photoelectron spectroscopy studies of these samples show that the silver particles are stable against oxidation in ambient air for periods of days (data not shown). SEM images (Philips x130) of the synthesized Ag nanoparticle arrays (Figure 1) show that the deposited Ag nanoparticles are generally spherical, narrowly dispersed in diameter, and spaced by 2−15 nm along each step. These 1D arrays are spaced laterally by several hundred nanometers. The average diameter of these nanoparticles measured along the rows is around 37 nm and the average spacing between two adjacent nanoparticles in the same row is about 7.5 nm. As shown in Figure 1b,c, the gaps between these nanoparticles can be very small, ∼1 or 2 nm and some nanoparticles are very close and almost connect with each other. Figure 1, panels d and e, presents the histograms of the particle width and the interparticle gap sizes shown in Figure 1c, respectively. The histograms indicate the distribution of the particle width and the interparticle gap sizes for this sample. Given the intrarow particle spacing is significantly smaller than the inter-row particle spacing, we assume the electromagnetic coupling between different particle rows is very weak and can be ignored. Only the nanoparticles in the same row strongly couple with the ones adjacent to them. This morphology provides an excellent platform for polarization-dependent SERS.

To characterize the polarization dependence, thiophenol was used as a probe molecule to explore the enhanced electromagnetic fields and the subsequent SERS around the silver nanoparticle arrays. Following the silver nanoparticle array synthesis outlined above, freshly made samples were submerged in freshly prepared 5 mM ethanolic (Rossville Gold Shield, 200 proof,

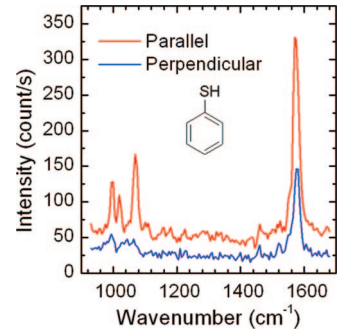

Figure 2. Enhanced Raman spectra of adsorbed thiophenol on silver nanoparticle arrays on the same HOPG substrate as shown in Figure 1. Red line and blue line correspond to the cases that the laser polarization is parallel and perpendicular to the direction of the nanoparticle arrays, respectively.

Hayward, CA) thiophenol (Aldrich ≥99%, used as received) solution for 3 h. In this process, a self-assembled monolayer of thiophenol was formed around the silver particles via S−Ag bonds.[21] Following the reaction period, samples were removed, copiously rinsed in ethanol, and dried in nitrogen gas to remove unreacted thiophenol and solvent. Macroscopic marks were made on the samples to correlate sampling areas as well as the nanoparticle array orientation in the SEM and Raman scattering experiments. For Raman experiments, a polarized 15 mW, 532 nm diode-pumped solid state laser beam passed through a stepper motor-controlled half-wave plate and was focused perpendicularly incident to the sample and focused onto a ∼15 μm diameter area. The backscattered light was directed through a depolarizer and collected by a SPEX monochromator (No. 1403, Horiba, NJ) with a photomutiplier tube (PMT). Both the monochromator and the stepper motor were controlled by LabView programs. In this experimental arrangement, we can measure the scattered Raman light independently as functions of incident polarization or Raman shift. After the polarized Raman experiments, the samples were imaged using SEM to obtain images such as those shown in Figure 1.

Figure 2 shows the enhanced Raman spectra from thiophenol adsorbed on the Ag nanoparticle arrays on the same HOPG substrate as shown in Figure 1. The three Raman peaks at 999, 1024, and 1073 cm^{-1} are assigned to the in-plane ring-breathing

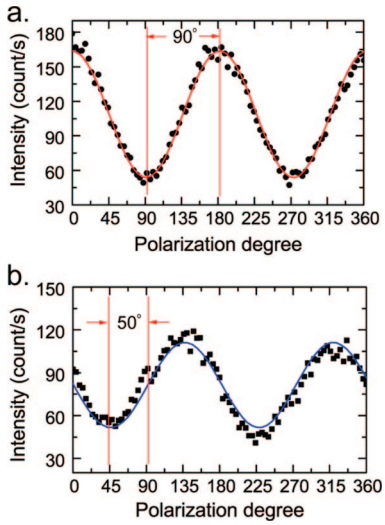

Figure 3. Polarization dependence of the enhanced Raman intensity of the band at 1073 cm^{-1}. The polarization angle of the incident radiation was rotated through 360° and the Raman intensity was recorded at 4° intervals (frame a) while the position of the silver nanoparticle arrays remained fixed. The experiment was repeated after rotating the nanoparticle array sample by 50°. Frame b indicates that the resulting intensity distribution is correspondingly shifted by 50°. Black dots and squares are experimental points and solid lines are fitted by $\cos^2$ function.

mode, the in-plane C−H bend, and the in-plane ring-breathing mode coupled to the C−S stretching mode, respectively.[22] The peak at 1572 cm^{-1} is due to the overlap of Raman signals from both thiophenol and HOPG substrate. Figure 2 also highlights the strong dependence on the polarization of the incident light. When the laser polarization is parallel to the nanoparticle rows, the Raman signals are very strong (red line). When the laser polarization is perpendicular to the nanoparticle rows, almost no Raman signals of thiophenol are observed (blue line). After subtracting the background, the signals from parallel polarization are approximately 20-fold stronger than what is from perpendicular polarization.

To achieve a better understanding of the polarization effects, the monochromator was set to record at the Raman peak 1073 cm^{-1}, while the incident laser polarization was scanned 360° in 4° intervals (Figure 3a, black dots). This change in Raman intensity was fitted well by a $\cos^2$ function (Figure 3a, red line) and indicates the difference between the maximum and minimum signals corresponding to a polarization rotation of 90°. As corroborated by the orientation in the SEM, the Raman signal reaches a maximum and minimum when the polarization is parallel and perpendicular to the nanoparticle rows, respectively. To verify that this effect results from the nanoparticle array orientation, the HOPG substrate with arrays of Ag nanoparticle rows was rotated by an angle 50°, resulting in a change in direction of the nanoparticle arrays by 50°. Figure 3b shows the resulting scattering intensities and a similar $\cos^2$ fit which indeed show a shift in the polarization dependence of the scattering intensities by the expected 50°.

The experimental Raman enhancement factor (EF) was evaluated for the case of parallel polarization by using eq 1.

$$\mathrm{EF} = (N_{\mathrm{ref}}/N_{\mathrm{SERS}})(I_{\mathrm{SERS}}/I_{\mathrm{ref}}) \quad (1)$$

where I_{SERS} and I_{ref} are the SERS intensity of thiophenol on Ag particle arrays and the normal Raman scattering intensity of a 120-μm thiophenol film in bulk, respectively, and N_{SERS} and N_{ref} are the number of thiophenol molecules adsorbed on the Ag arrays within the laser spot area and the number of thiophenol molecules in the film to obtain the corresponding normal Raman spectra, respectively. Taking the sampling area (15 μm in diameter), the silver particle coverage (~9% of the HOPG surface), and the equilibrated surface concentration of thiophenol ($\sim 3.0 \times 10^{14}$ molecules/cm^2)[23] into account, N_{SERS} is equal to 4.8×10^7. When taking the reference spectrum of pure thiophenol, the sampling volume is the 120-μm film penetrated by the Gaussian laser beam with 15 μm diameter. N_{ref} is calculated to be 1.3×10^{14} as the density of pure thiophenol is 1.08 g cm^{-3}. When I_{SERS} and I_{ref} were measured at 1073 cm^{-1}, the Raman intensity ratio, $I_{\mathrm{SERS}}/I_{\mathrm{ref}}$, is 0.04 and the enhancement factor is $\sim 1.1 \times 10^5$.

Theoretical calculations of the electromagnetic response of coupling Ag nanoparticles to a light source enable a quantitative understanding of the polarized SERS results. These calculations model the surface electric fields due to surface plasmons interacting with the applied electromagnetic radiation. Surface plasmons among the Ag particles are a localized resonant mode of electromagnetic fields. The plasmon resonance frequency in general depends on the dielectric properties of the metallic nanostructure and the embedding medium while the sensitivity of this dependence is a function of nanostructure size and geometry.[24–26] Localized surface plasmons among the Ag nanoparticles dramatically enhance the electromagnetic field, which excites molecules adhered to the surface of the Ag particles. The radiation scattered by the particle will via a host of processes such as interband transitions also overlap with the Raman shifted wavelength and actively drive the emission process. As a result, the intensity of the Raman scattering is proportional to the fourth power of the enhancement of the local electromagnetic field.[27] Thus, it is instructive to explore the enhanced fields around the Ag nanoparticles and the effects of array morphology.

Since the molecules responsible for the largest signals are located near the two poles of adjacent spheres at the point of minimum distance between them, the essential features of the enhanced fields can be captured by considering simply a pair of Ag spheres. As shown in Figure 4a, we consider two Ag spheres with radius R separated by a distance d along the z-axis in the medium of air. For comparison to the experimental result, R was chosen as the average radius of Ag particles for the sample used to obtain the spectra shown in Figure 2, which is 18.6 nm. Polarized light with wavelength of 532 nm is perpendicularly incident to the $x-z$ plane. Figure 4b shows the square of the enhanced field at the surface of the top sphere as a function of θ for both z and x-polarized incident light when the gap between the spheres is 1 nm. The enhanced field is normalized to the value of the incident light field far from the pair of spheres. When the incident light is polarized along the z direction, corresponding to linear polarization parallel to the intersphere axis, the square of the field enhancement can be as high as above 4000. The strongest field position on the top sphere shown in Figure 4a is at the south pole which corresponds to $\theta = \pi$. The strongly enhanced field only extends over a small angular range. When the incident light is polarized along the x direction, corresponding to polarization perpendicular to the intersphere axis, the strongest field appears at $\theta = \pi/2$ or $3\pi/2$ and the enhanced field extends over a much larger angular range. However, in this case the maximum enhancement in the square of the field is only around 10. It is clear that the field enhancement in the case of parallel polarization incident radiation is significantly stronger than the enhancement for perpendicular polarization incidence, which is consistent with

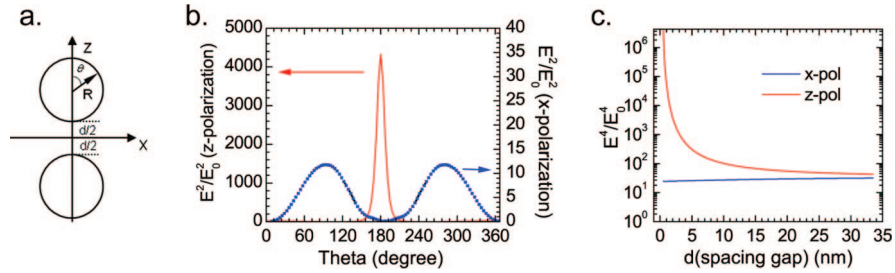

Figure 4. Theoretical model for electric field enhancements due to plasmon resonance. Figure 4a indicates the two-sphere geometry for the calculation with $R = 18.6$ nm and a gap of 1 nm. Frame b plots the normalized square of the field at the surface of the sphere versus θ for both z (red) and x-polarized (blue) incident radiation fields. This indicates exceptionally enhanced fields between the particles when incident light is aligned parallel to the interparticle axis. Frame c shows the average fourth power field around one of the two Ag spheres as a function of particle separation, d, for both z- (red) and x-polarized (blue) incident radiation fields.

our experimental findings shown in Figure 2. The origin of this difference lies in the fact that, for perpendicular excitation, the collective plasmon mode excited by a uniform field is blue-shifted substantially relative to that excited in parallel polarization.

According to Figure 4b, the field is not uniformly distributed over the spheres, so the experimentally acquired Raman signals do not result equally from the thiophenol molecules adsorbed throughout the surface of the nanoparticles. Since enhanced Raman signals are proportional to the fourth power of the field enhancement, the average of the fourth power of the field enhancement over the sphere surface presents a more appropriate evaluation of the Raman enhancement factor. From the theoretical model discussed above, Figure 4c plots the average fourth power of the field enhancement around one of the two spheres as a function of particle separation d for both z (red) and x-polarized (blue) incident light. The field enhancement greatly depends on the separation for z-polarized incident light as the fourth power of the field enhancement decreases rapidly from $>10^6$ for $d = 1$ nm to below 100 for $d > 10$ nm. When the incident light is polarized along the x axis, the field enhancement is not as strongly coupled to particle spacing as it is for z-polarized light. Interestingly, as the separation gets larger, the field enhancement becomes slightly stronger for the x-polarized light. When the separation goes above 30 nm, the field enhancements are virtually identical for x and z-polarized incident light. That is as expected since when the separation is large enough, the two-particle system effectively becomes two independent one-particle systems that exhibit no polarization dependence.

As the E^4 enhancement depends on gap sizes, the distribution of particle gaps shown in Figure 1 contribute differently to the overall Raman scattering signal. To ascertain the cumulative effect of the various gap sizes, the average of the fourth power of the field enhancement around the sphere is averaged over the experimentally determined gap size distribution in Figure 1e. This weighted average gives a good evaluation of the average experimental electromagnetic enhancement. The calculated average electromagnetic enhancement factors for z- and x-polarized incident light are 5013 and 27, respectively. Considering the chemical enhancement for Raman signals is on the order of 10^2,[28] the total Raman enhancement factor is $\sim 5 \times 10^5$ for z-polarized incident light which is the same order as the experimental enhancement factor 1.1×10^5. The experimental enhancement factors obtained are the average enhancement factors which mean they are averaged over the whole surface of all the Ag particle arrays and all the different gap sizes, which explains why they are much lower compared to the enhancement factor of $\sim 10^{14}$ for hot spots.[2,3] From Figure 4b, we can see the hot spot is located at the gap area between the particles. If we do not average the calculated electromagnetic enhancement over the whole particle, it can be as high as 10^{10} at the gap area for a gap size of 0.5 nm.

According to the calculations, the Raman enhancement for z-polarized incident light is about 200 times stronger than the enhancement for x-polarized incident light. However, Figure 2 only indicates a 20-fold ratio between scattering from z- and x-polarized light. One reason for the smaller than expected polarization effect is the existence of a small number of particle rows with an inter-row spacing comparable to the 10 nm spacing between particles within an individual row. Such closely spaced rows would be expected to contribute significantly to enhanced scattering from x-polarized light. As we mentioned previously, our theoretical calculations assumed no coupling between the rows of particles.

In summary, we demonstrate the PVD fabrication of highly ordered Ag nanoparticle arrays on HOPG substrates. Strong polarized SERS has been observed from molecules adsorbed on these arrays. Electromagnetic calculations performed are consistent with our experimental results. Ongoing studies include controlling the Ag particle and gap sizes by changing evaporation parameters such as evaporation rate, time, and substrate temperature. We anticipate this PVD method would give us more capability in fabricating efficient SERS substrates.

Acknowledgment. This work was supported by grants from the DOE Office of Basic Energy Sciences DE-FG02-96ER45576 and DE-FG03-84ER-45083 and by NSF DMR-0654055. The work was also supported by the UCI School of Physical Sciences Center for Solar Energy. We acknowledge the UCI Material Characterization Center for the use of the SEM facility.

References and Notes

(1) Jeanmaire, D. L.; Van Duyne, R. P. *J. Electroanal. Chem.* **1977**, *84*, 1.
(2) Nie, S.; Emory, S. R. *Science* **1997**, *275*, 1102.
(3) Kneipp, K.; Wang, Y.; Kneipp, H.; Itzkan, I.; Dasari, R. R.; Feld, M. S. *Phys. Rev. Lett.* **1996**, *76*, 2444.
(4) Hu, J.; Zhao, B.; Xu, W.; Fan, Y.; Li, B.; Ozaki, Y. *Langmuir* **2002**, *18*, 6839.
(5) Suzuki, M.; Niidome, Y.; Kuwahara, Y.; Terasaki, N.; Inoue, K.; Yamada, S. *J. Phys. Chem. B* **2004**, *108*, 11660.
(6) Xu, H.; Käll, M. *Chem. Phys. Chem.* **2003**, *4*, 1001.
(7) Suzuki, M.; Maekita, W.; Wada, Y.; Makajima, K.; Kimura, K.; Fukuoka, T.; Mori, Y. *Appl. Phys. Lett.* **2006**, *88*, 203121.
(8) Jeong, D. H.; Zhang, Y. X.; Moskovits, M. *J. Phys. Chem. B* **2004**, *108*, 12724.
(9) Tao, A. R.; Yang, P. *J. Phys. Chem. B* **2005**, *109*, 15687.
(10) Brolo, A. G.; Arctander, E.; Addison, C. J. *J. Phys. Chem. B* **2005**, *109*, 401.
(11) Nordlander, P.; Oubre, C.; Prodan, E.; Li, K.; Stockman, M. I. *Nano Lett.* **2004**, *4*, 899.

(12) Brandl, D. W.; Oubre, C.; Nordlander, P. *J. Chem. Phys.* **2005**, *123*, 024701.
(13) Wang, H.; Levin, C. S.; Halas, N. J. *J. Am. Chem. Soc.* **2005**, *127*, 14992.
(14) Lee, S. J.; Morrill, A. R.; Moskovits, M. *J. Am. Chem. Soc.* **2006**, *128*, 2200.
(15) Shegai, T. O.; Haran, G. *J. Phys. Chem. B* **2006**, *110*, 2459.
(16) Jiang, J.; Bosnick, K.; Maillard, M.; Brus, L. *J. Phys. Chem. B* **2003**, *107*, 9964.
(17) Etchegoin, P. G.; Galloway, C.; Le Ru, E. C. *Phys. Chem. Chem. Phys.* **2006**, *8*, 2624.
(18) Itoh, T.; Hashimoto, K.; Ozaki, Y. *Appl. Phys. Lett.* **2003**, *83*, 2274.
(19) Cross, C. E.; Hemminger, J. C.; Penner, R. M. *Langmuir* **2007**, *23*, 10372.
(20) Francis, G. M.; Kuipers, L.; Cleaver, J. R. A.; Palmer, R. E. *J. Appl. Phys.* **1996**, *79*, 2942.
(21) Laibinis, P. E.; Whitesides, G. M.; Allara, D. L.; Tao, Y. T.; Parikh, A. N.; Nuzzo, R. G. *J. Am. Chem. Soc.* **1991**, *113*, 7152.
(22) Joo, T. H.; Kim, M. S.; Kim, K. *J. Raman. Spectrosc.* **1987**, *18*, 57.
(23) Gui, J. Y.; Stern, D. A.; Frank, D. G.; Lu, F.; Zapien, D. C.; Hubbard, A. T. *Langmuir* **1991**, *7*, 955.
(24) Hicks, E. M.; Zou, S.; Gunnarsson, L.; Rindzevicius, T.; Käll, M.; Kasemo, B.; Schatz, G. C.; Spears, K. G.; Van Duyne, R. P. *Nano lett.* **2005**, *5*, 1065.
(25) Hao, E.; Schatz, G. C. *J. Chem. Phys.* **2004**, *120*, 357.
(26) Xu, H.; Aizpurua, J.; Käll, M.; Apell, P. *Phys. Rev. E* **2000**, *62*, 4318.
(27) Moskovits, M. *J. Raman Spectrosc.* **2005**, *36*, 485.
(28) Udagawa, M.; Chou, C. C.; Hemminger, J. C.; Ushioda, S. *Phys. Rev. B* **1981**, *23*, 6843.

JP803455S